Journal of Energy

VOLUME 74 Number 2 | 2025

journal homepage: http://journalofenergy.com/

Experimental Investigation of Critical Heat Flux and Post-Critical Heat Flux in a Carbon Dioxide-Cooled Tube at High Subcritical Pressures

Jakub Bronik, Michael Buck, Jörg Starflinger

***Summary* — Supercritical fluids such as water or CO_2 are an attractive choice for future nuclear reactor systems. The exact knowledge of the heat transfer in a trans-critical pressure is important for the design of those systems. In subcritical pressure, knowing how to avoid the reduction of heat removal when exceeding the critical heat flux (CHF) is of critical importance.**

A series of experiments is carried out with the SCARLETT (Supercritical CARbon dioxide Loop at IKE StuTTgart) test facility at the Institute of Nuclear Technology and Energy Systems of the University of Stuttgart, focusing on investigations of CHF and post-CHF heat transfer with CO_2 as a working fluid. Two test sections have been used – each with a different internal diameter - to investigate CHF and post-CHF heat transfer. Both test sections with 10 mm and 6 mm internal diameters and heated lengths of 2000 mm are equipped with glass fiber in a stainless-steel capillary for semi-continuous wall temperature measurement and thermocouples for the reference temperature measurement. The test sections are instrumented accordingly for pressure, differential pressure, mass flow, inlet, and outlet temperature measurements. The paper presents CHF, upstream CHF, and boiling heat transfer measurements in selected experiments in the 10mm tube at subcritical pressures of pr=0.7 and pr=0.98, mass fluxes of 1000 kg/m2s, and heat fluxes from 80 to 200 kW/m2.

***Keywords* — CHF, post-CHF, dryout, OFDR, boiling**

I. Introduction

In transient operations of thermal cycles designed to operate at a supercritical state, pressure may pass the critical pressure and thus lead to a transition between supercritical and subcritical states under normal or abnormal conditions. Reliable models for heat transfer in both supercritical and subcritical states therefore, play an important role in safety design and safety analysis.

Figure 1 shows schematically the heat transfer in two-phase flow using the boiling curve, which represents the heat flux as a function of the superheat of the heated wall. At low heat flux, nucleate boiling takes place on the heated wall. However, if the heat flux continues to increase and reaches a critical value, direct contact between the liquid and the heated wall is lost, and heat transfer is significantly reduced. If the imposed heat flux remains constant, the regime changes from bubble boiling to film boiling, and the wall temperature increases significantly. This phenomenon is called boiling crisis, and the corresponding heat flux is called critical heat flux (CHF). The regime after the appearance of the boiling crisis is called post-CHF. Even if the heat flux is reduced after the occurrence of the boiling crisis, the flow regime remains in the film boiling (post-CHF region) until the wall temperature falls below the so-called minimum film boiling temperature (Leidenfrost point). Then the wall is wetted again with liquid and a sudden drop in the wall temperature occurs. This process is called rewetting.

Heat transfer in the subcritical pressure state, including post-CHF heat transfer, has been studied very intensively in the past for reduced pressures up to p/pcrit≤0.7 (ratio referred to as p_r), also because of its importance in light water reactors [1]. There exists a large number of models or correlations developed for this pressure range.

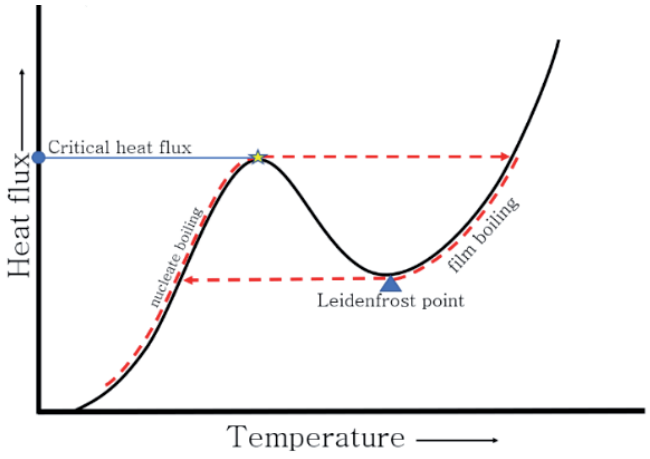

Fig. 1. Boiling curve.

However, studies of heat transfer under subcritical pressure conditions but in the high-pressure range $0.7<p_r<1$ have been scarce [2], and correspondingly, the theoretical prediction models lack validation and are only applicable for a limited range of conditions. E.g., analysis of the transient processes in a 4-rod bundle with water cooling showed that the thermohydraulic system code ATHLET cannot satisfactorily predict heat transfer in the high-

Corresponding author: Jakub Bronik

Jakub Bronik, Michael Buck and Jörg Starflinger are with the University of Stuttgart, Institute of Nuclear Technology and Energy Systems, Stuttgart, Germany

(emails: jakub.bronik@ike.uni-stuttgart.de, michael.buck@ike.uni-stuttgart.de, jorg.starflinger@ike.uni-stuttgart.de)

Jakub Bronik, Michael Buck, Jörg Starflinger, Experimental Investigation of Critical Heat Flux and Post-Critical Heat Flux in a Carbon Dioxide-Cooled Tube at High Subcritical Pressures, Journal of Energy, vol. 74 Number 2 (2025), 3–7
https://doi.org/10.37798/2025742716

pressure range [3]. The experiment showed that during the transient process with decreasing pressure from 25 MPa to 17 MPa, a sharp increase in wall temperature occurs at a pressure of about 21 MPa. This corresponds to the appearance of the boiling crisis, which, however, was not predicted by the ATHLET code.

The present paper concentrates on the experimental investigations to improve the knowledge about the physical processes of heat transfer at subcritical pressures near the critical point and in the adjacent post-CHF range.

II. Experimental Setup

All experiments presented in this publication were carried out in the SCARLETT (Supercritical Carbon dioxide Loop at IKE Stuttgart) test facility at IKE. SCARLETT works as a peripheral facility used to provide CO_2 under defined parameters: mass flow rate, temperature, and pressure near the critical point. Detailed information about SCARLETT is available in Flaig et al. [4]. While SCARLETT has been used in the past mostly to work at supercritical pressure, the facility has been modified for the present experiments to safely operate in subcritical pressures. This was achieved by the implementation of a reduction valve upstream of the test section. A simplified schematic is presented in Fig. 2.

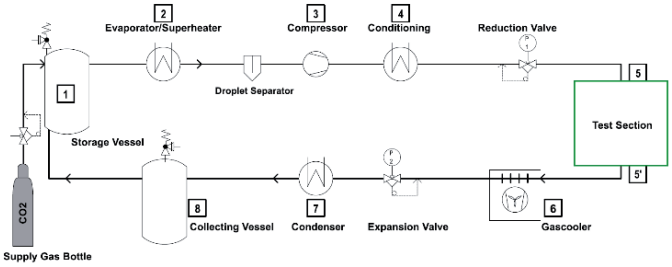

Fig. 2. SCARLETT schematic.

For the investigations presented in this publication, two different test sections have been used, with 6 mm, and 10 mm inner diameters. Another diameter was chosen due to the convenience of obtaining the pipes. The 6 mm and 10mm test sections can be seen in Figure 3. The test sections were operated in parallel, which has the advantage that the mass flow rate through each test section can be adjusted by diverting flow through the other test section. The test sections have the same structure; the only difference is the diameter of the test tubes used. The test tubes are heated directly with a 35 kW DC power supply. To insulate the test rig electrically from the test tubes, special insulating flanges are used. The mass flow rate and bulk temperature of the CO_2 are measured just before the entry into the test sections. Fig. 3 shows the dimensions of the test tubes with an inner diameter of 6 and 10 mm and an outer diameter of 8 and 12 mm. The material of the tubes is Alloy 625.

The total length of the test tubes is 2533 mm with a heated length of 2000 mm. The tubes are instrumented with glass fiber in a stainless-steel capillary for temperature measurement. As a reference and for calibration purposes, 20 T-type thermocouples are tied with a temperature-resistant yarn straight in 100 mm intervals on the outer surface of the test tube adjacent to the capillary. Both thermocouples and capillary have been electrically insulated from the pipe with a 200 µm thick mica paper layer. The absolute pressure is measured before and after the heated section, and the differential pressure is measured over the heated length. The pressure inside the test tube is measured through a 1 mm hole to avoid influencing the flow – the setup can be seen in Figure 3 on the bottom right. A more detailed description can be found in [5].

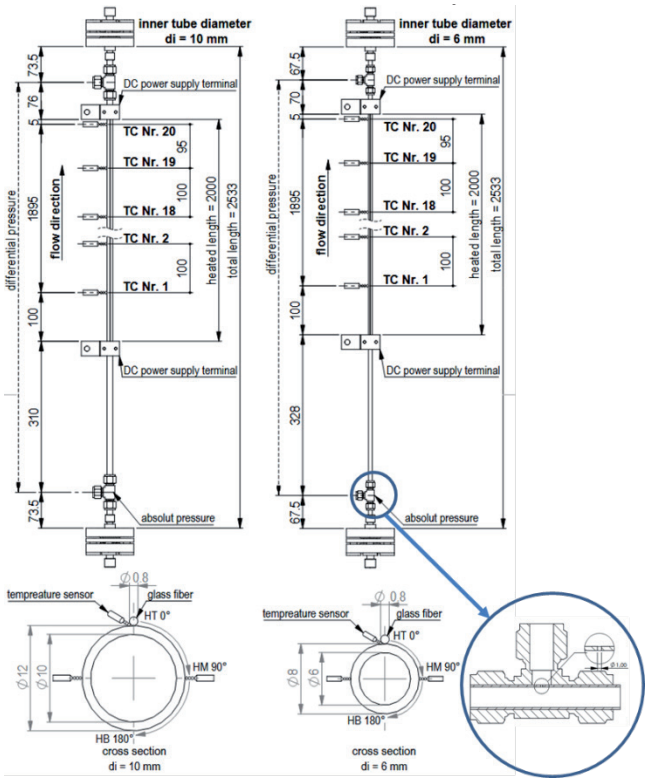

Fig. 3. Test section and pressure tapping.

A. Glass Fiber Setup

The relationship between the relative changes of wavelength λ and frequency f, temperature T, and strain ε is approximately linear, as eq. (1) below indicates. The coefficients KT and Kε depend on the material and can vary by up to 10% between standard telecom glass fibers.

$$\frac{\Delta\lambda}{\lambda} = -\frac{\Delta f}{f} = K_T\,\Delta T + K_\varepsilon\,\varepsilon \tag{1}$$

For a strain-free measurement, equation (1) can be transformed into equation (2) to provide the temperature change as a linear function of the measured frequency change [6].

$$\Delta T = -\frac{\bar{\lambda}}{c_0\,K_T}\,\Delta f \tag{2}$$

For measurements over broader temperature ranges and/or for considering fiber-coating interactions [6], nonlinear fits to the correlation between temperature and frequency, e.g., using more accurate polynomials [7]. The relation between temperature and frequency changes was approximated by a second-order polynomial according to equation (3) for the fiber used in this setup.

$$\Delta T = -A\Delta f^2 + B\Delta f + C \tag{3}$$

The coefficients A, B, and C given in Table 1 below were determined by fitting the polynomial (3) to the measurements of the type T thermocouples.

Jakub Bronik, Michael Buck, Jörg Starflinger, Experimental Investigation of Critical Heat Flux and Post-Critical Heat Flux in a Carbon Dioxide-Cooled Tube at High Subcritical Pressures, Journal of Energy, vol. 74 Number 2 (2025), 3–7
https://doi.org/10.37798/2025742716

TABLE 1.

GLASS FIBER TEMPERATURE FIT COEFFICIENTS.

10 MM	A	-9.51E-07	B	9.51E-02	C	2.625E+01
6 MM	A	-1.43E-06	B	9.64E-02	C	2.7175+01

III. EVALUATION METHODOLOGY

Table 2. gives an overview of the measured parameter ranges.

TABLE 2.

EXPERIMENTAL OVERVIEW

Parameter [Unit]	Value
Inner tube diameter [mm]	10
Flow direction [-]	upward flow
Inlet pressure [MPa]	5.2, 7.2
Inlet temperature [°C]	8
Mass flux [kg/m²s]	1000
Heat flux [kW/m²]	80-200

In the following, a short overview of the calculations of the main variables is given. The National Institute of Science and Technology (NIST) database REFPROP provides the fluid properties [8].

$$\dot{Q}_{th} = P_{el} = U \cdot I \tag{4}$$

Heat flow rate $\dot{Q}_{th}$ gained by the fluid was calculated from the electric power P_{el} with the voltage U and the current I.

The heat flux $\dot{q}$ is calculated with the curved surface area of the inner surface A_i of the tube and the heated length with the assumption of a uniform heat generation by direct electrical heating, the heated length L_h, and internal diameter d_i.

$$\dot{q} = \frac{\dot{Q}_{th}}{A_i} = \frac{U \cdot I}{\pi \cdot d_i \cdot L_h} \tag{5}$$

For the calculation of the bulk temperature $T_{b,y}$ across the axial position of the tube y, a linear approximation of the pressure losses is assumed. Specific enthalpy at the axial position $i_{b,y}$ is calculated with enthalpy at inlet conditions $i_{b,in}$ and mass flow $\dot{m}$.

$$T_{b,y} = \mathrm{f}(i_{b,y}, p_y) \tag{6}$$

$$i_{b,y} = i_{b,in} + \left(\frac{y}{L_h}\right) \cdot \frac{\dot{Q}_{th}}{\dot{m}} \tag{7}$$

With the mathematical heat conduction model of a circular tube with uniform heat generation, an insulated outer surface, and a cooled inner surface, the inner wall-temperature $T_{w,i}$ can be calculated with the measured outer wall-temperature T_{625} and the volumetric heat flux $\dot{q}_v$ [9, p.152] and outer diameter d_o. The thermal conductivity λ_{625} of Alloy 625 was also approximated linearly over the temperature $\lambda_{625} = \mathrm{f}(T_{w,o})$.

$$T_{w,i} = T_{w,o} + \frac{\dot{q}_v}{4\lambda_{625}}\left[\left(\frac{d_o}{2}\right)^2 - \left(\frac{d_i}{2}\right)^2\right] - \frac{\dot{q}_v}{2\lambda_w}\left(\frac{d_o}{2}\right)^2 \cdot \ln\left(\frac{d_o}{d_i}\right) \tag{8}$$

$$\dot{q}_v = \frac{\dot{Q}_{th}}{\frac{\pi}{4}\left({d_o}^2 - {d_i}^2\right) \cdot L_h} \tag{9}$$

The inner wall temperature wall calculation has been repeated with the thermal conductivity of the tube at the mean wall temperature $\lambda_{625} = \mathrm{f}(\overline{T_{w.m}})$, where:

$$\overline{T_{w,m}} = \frac{T_{w,i} + T_{w,o}}{2} \tag{10}$$

In the last step, the heat transfer coefficient htc can be calculated for each temperature measurement point across the tube's axial position.

$$htc_y = \frac{\dot{q}}{T_{w,i,y} - T_{b,y}} \tag{11}$$

IV. RESULTS

Figure 4 shows the axial profiles of the wall temperature along the 10mm tube at p_r = 0.7 (52 bar) and at p_r = 0.98 (72 bar) for different values of heat flux up to 130 kW/m², 8°C inlet fluid temperature, and 1000 kg/m²s mass flux. The calculated bulk fluid temperature at the plot represents the values obtained for the highest heat flux at the plot.

The temperature profiles for the 52 bar were obtained after reaching the critical heat flux in a power ramp up (temperature excursion at the end of the heated length at 105±1.2 kW/m²) and fur-

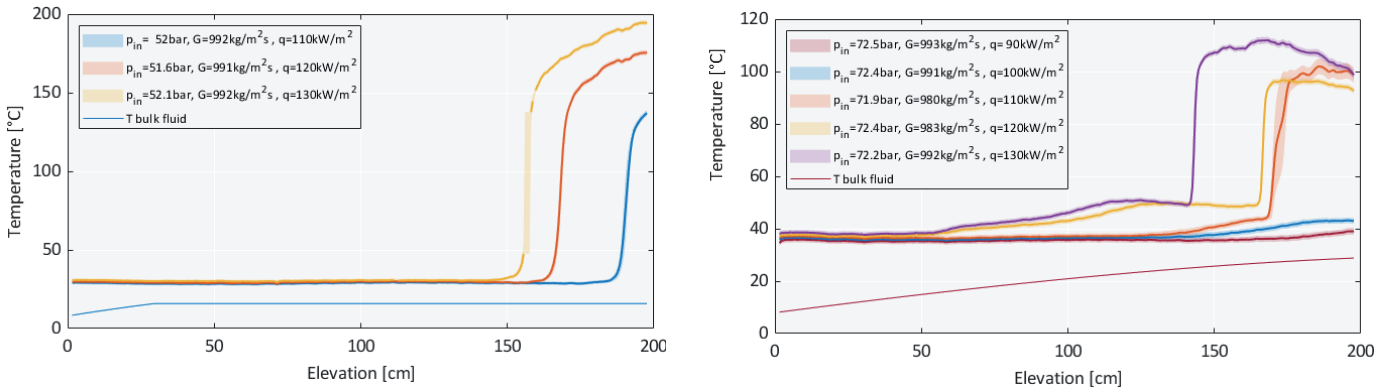

Fig. 4. Temperature profiles at increasing heat flux up to 130 kW/m² at p_r=0.7 and pr=0.98. T_{in}=8°C and G=1000 kg/m²s.

Jakub Bronik, Michael Buck, Jörg Starflinger, Experimental Investigation of Critical Heat Flux and Post-Critical Heat Flux in a Carbon Dioxide-Cooled Tube at High Subcritical Pressures, Journal of Energy, vol. 74 Number 2 (2025), 3–7
https://doi.org/10.37798/2025742716

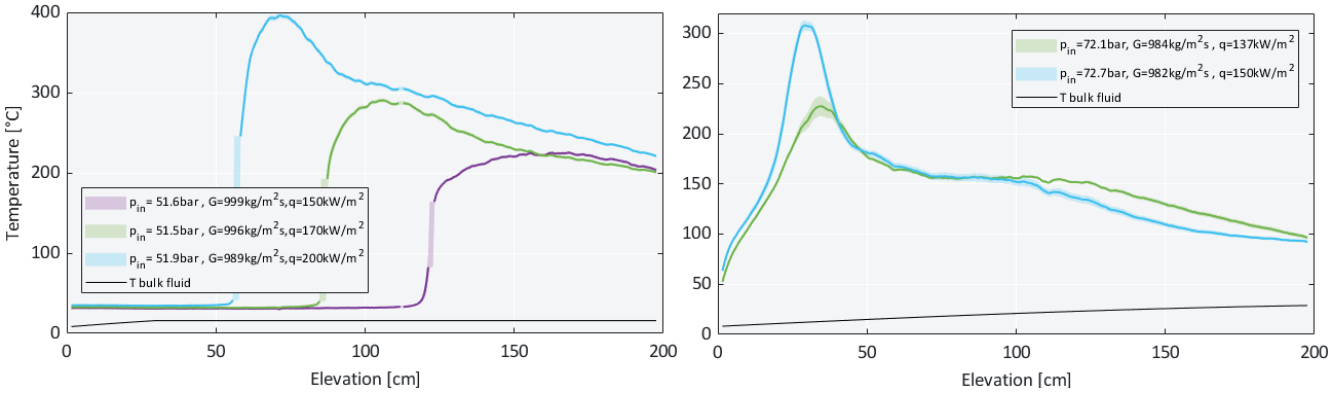

Fig. 5. Temperature profiles at increasing heat flux above 130 kW/m² at p_r=0.7 and p_r=0.98. T_{in}=8°C and G=1000 kg/m²s

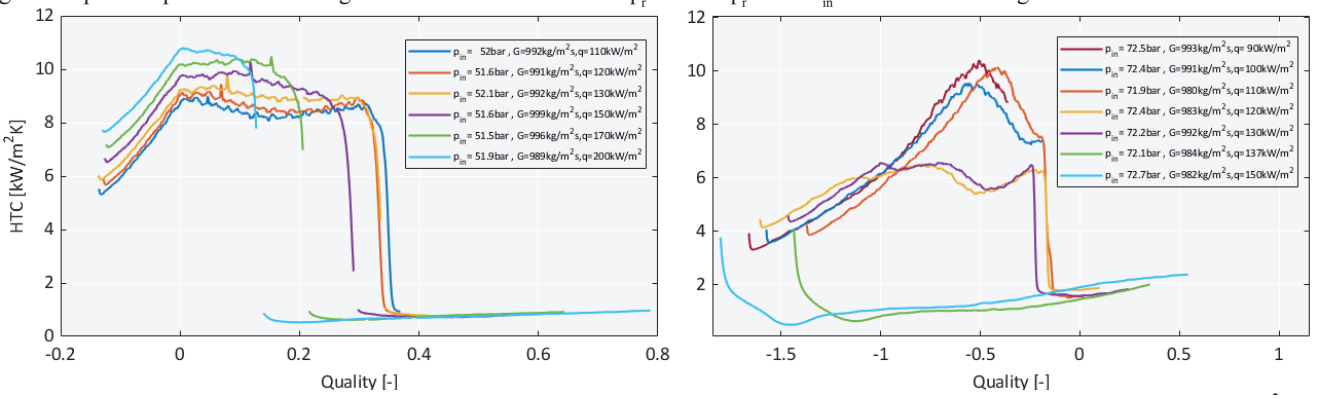

Fig. 6. Heat transfer coefficients in relation to equilibrium quality at increasing at p_r=0.7 and p_r=0.98. T_{in}=8°C and G=1000 kg/m²s.

ther raise of the heating power to obtain post-CHF conditions. The power was kept constant for a sufficiently long period to produce a sequence of steady-state conditions. Detailed description of data recording, averaging, and methodology can be found in [5].

The position of the steep temperature increase corresponds to the CHF point; the CHF conditions have to be taken as the local conditions at the jump position, which defines a "virtual" end of the heated length. At the presented heat fluxes, the post-steep increase profiles exhibit an inclined shape, suggesting the main heat transfer interaction to be heat transfer between the wall and the heated vapor in post-CHF, where the near-wall vapor is gradually superheated.

The temperature profiles at 72 bar were obtained similarly; however, there were two indications of a jump-wise temperature increase at the end of the heated length (first at 86±0.8 kW/m², second at 105±0.5 kW/m²). The profiles obtained after the first CHF-like-event indication (at 90 and 100 kW/m²) show a mild temperature increase of about 8°C compared to the wall temperature at nucleate boiling upstream of the tube. This first temperature jump

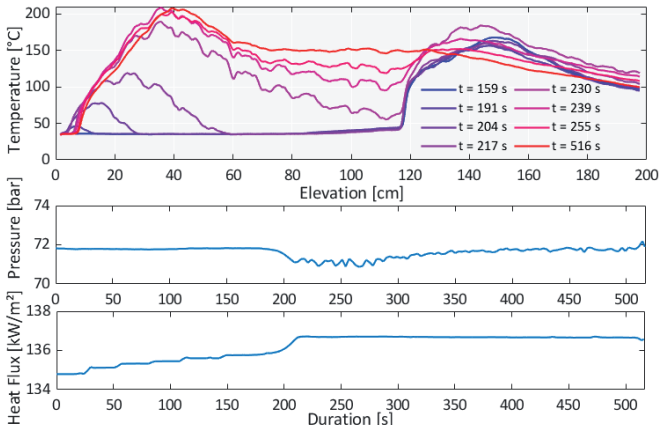

Fig. 7. Development of temperature profile at upstream CHF.

is present at each superheating and is interpreted to be some sort of unstable boiling due to froth flow or dry patching, rather than CHF. The second temperature jump in the profiles with 110, 120, and 130 kW/m² is much larger (>50°C). The plateau shape of those profiles after the location of CHF suggests a stable temperature of vapor. At 130 kW/m² there is a small decrease of temperature at the end of the heated length – this indicates a stronger influence of droplet evaporation, as vapor picks up speed. The maximum wall temperatures obtained in those experiments are much lower when compared to the ones in corresponding cases in 52 bar.

Figure 5 presents the results of overheating the pipe at both pressures above 130 kW/m². The profiles at 52 bar show the evolution in shape from inclined lines at the previous plot to a convex shape with a maximum at 150 kW/m². There, the superheated steam reaches equilibrium, and the main heat transfer mechanism becomes the evaporation of droplets from superheated vapor, leading to an increase in the vapor speed. The following profiles have a temperature peak in the first half of the heated length – indicating a change of CHF mechanism from dryout to DNB – where due to violent change to reverse annular boiling the wall temperature rises, the main heat transfer mechanism becomes radiation from wall to liquid core and its evaporation – leading to speed up of vapor at the wall until it reaches equilibrium state.

At the pressure of 72 bar the temperature profiles change drastically due to the occurrence of upstream CHF, a CHF mechanism taking place in the middle or the beginning, believed to happen due to the change of flow pattern [9, 10, 11]. It results in a spike-like peak of temperature and temperature profile development up the stream, similar to the post-DNB case. In this case, nucleate boiling does not happen anywhere along the heated length. It has to be noted that the wall superheat at the hottest point in the 150 kW/m² case is 100 K higher than the hottest temperature at a corresponding case at 52 bar. The power was not further increased to avoid damaging the test section.

Figure 7 shows the evolution of the temperature profile upon passing the upstream CHF value – the small peak in temperature at

Jakub Bronik, Michael Buck, Jörg Starflinger, Experimental Investigation of Critical Heat Flux and Post-Critical Heat Flux in a Carbon Dioxide-Cooled Tube at High Subcritical Pressures, Journal of Energy, vol. 74 Number 2 (2025), 3–7
https://doi.org/10.37798/2025742716

the beginning of the heated channel at t = 191s evolves in a matter of 42 seconds to reach maximum temperature. It has to be noted that at the beginning of the process, both temperature peaks – due to classical and upstream CHF – increase. Starting at t = 239 s, the peak due to classical CHF starts to diminish. Upstream CHF is followed by a disturbance in test section pressure due to flow regime change and a slight increase of heated power, due to drastic temperature change on the whole heated length and significant increase of its electrical resistance.

Figure 6 shows the heat transfer coefficients calculated from the corresponding experiments at Figures 4 and 5 in relation to equilibrium quality. In case of the experiments at 52 bar all the CHF events happened at a positive quality, indicating usual two-phase flow regimes, and in case of experiments at 110-130 kW/m^2, a dryout mechanism of CHF. At 72 bar, as the CHF always happens at subcooled conditions, the CHF mechanism has to be DNB. It should be noted as well that the first degradation of heat transfer leads to a 20% decrease in the heat transfer coefficient.

V. Conclusions

A series of experiments at p_r = 0.7 and p_r = 0.98 has been performed. At lower reduced pressures, CHF happened solely at positive qualities, while at close critical pressure, it happened only in subcooled conditions. While at high pressures, a pre-CHF heat transfer deterioration happened, the wall temperatures in the post-CHF regime were lower than in corresponding p_r = 0.7 experiments. This improved performance is, however, limited by the possibility of upstream CHF, which is due to a heavy decrease of the heat transfer coefficient that is even lower than in the presented post-DNB cases.

VI. References

[1] D. Yu, F. Feuerstein, L. Köckert, X. Cheng, "Analysis and modelling of post-dryout heat ransfer in upward vertical flow", Ann. Nucl. Energy vol. 115, pp 186-194, May 2018

[2] D.B. Marchetto, "A state-of-the-art review on flow boiling at high reduced pressures", Int.J. Heat Mass Transf., Vol. 193, 2022

[3] M. Q. Song, X. J. Liu, X. Cheng, "Heat transfer analysis of trans-critical pressure transient, Annual Meeting of Nuclear Engineering", Berlin, Germany, May 7-8, 2019.

[4] W. Flaig, "Setup of the supercritical CO2 test facility SCARLETT for basic experimental investigations of a compact heat exchanger for an innovative decay heat removal system", J. Nucl. Eng. Radiat. Sci., 4 (3) (2018)

[5] J Bronik et al. 'Experimental investigation of critical heat flux and post-critical heat flux in a carbon dioxide-cooled tube at high subcritical pressures', NUTHOS 14, Vancouver, Aug 25-28 2024

[6] A.K. Sang et al. "One Centimeter Spatial Resolution Temperature Measurements in a Nuclear Reactor Using Rayleigh Scatter in Optical Fiber". IEEE Sens.J., vol.8, p1375–1380, 2008.

[7] Luna Innovations Incorporated, Distributed Fiber Optic Sensing: Temperature Coefficient for Polyimide Coated Low Bend Loss Fiber, in the 10°C - 80°C Range, Blacksburg, 2014.

[8] REFPROP, NIST SRD 23, USA, 2010

[9] Kitto, J. B., "Upstream Critical Heat Flux and Its Design Implications". Heat Transf. Eng, 43(6), 475–484, 2021

[10] D. C. Groeneveld, "The occurrence of upstream dryout in uniformly heated channels," Proc. 5th Inter. Heat Transfer Conf., Tokyo, Japan, Sept. 3–4, 1974,vol. 4, pp. 265–269

[11] Y. Katto and S. Yokoya, "CHF of force convection boiling in uniformly heated vertical tubes: Experimental study of HP-regime by the use of refrigerant 12," Int. J. Multiphase Flow, vol. 8, no. 2, 165–181, Apr. 1982